Electronic Supplementary Material (ESI) for RSC Applied Polymers.

Supporting information of the manuscript entitled: Assessing the Performance of Sustainable Luminescent Solar Concentrators based on Chemically Recycled Poly(methyl methacrylate)

Alberto Picchi,[a] Irene Bettini[b], Massimo Ilarioni[b], Marco Carlotti,[a,c] Andrea Pucci,[a,,c,d]

[a]Department of Chemistry and Industrial Chemistry, University of Pisa, Via Giuseppe Moruzzi 13, 56124 Pisa, Italy

[b]I&S srl, Via F.lli Chiaruffi 12, 50067 Rignano sull'Arno, Florence, Italy

[c]CISUP, Centro per l'Integrazione della Strumentazione dell'Università di Pisa, Lungarno Pacinotti 43, 56126 Pisa, Italy

[d]INSTM UdR of Pisa, University of Pisa, Via Giuseppe Moruzzi 13, 56124 Pisa, Italy

Gas chromatographic analyses

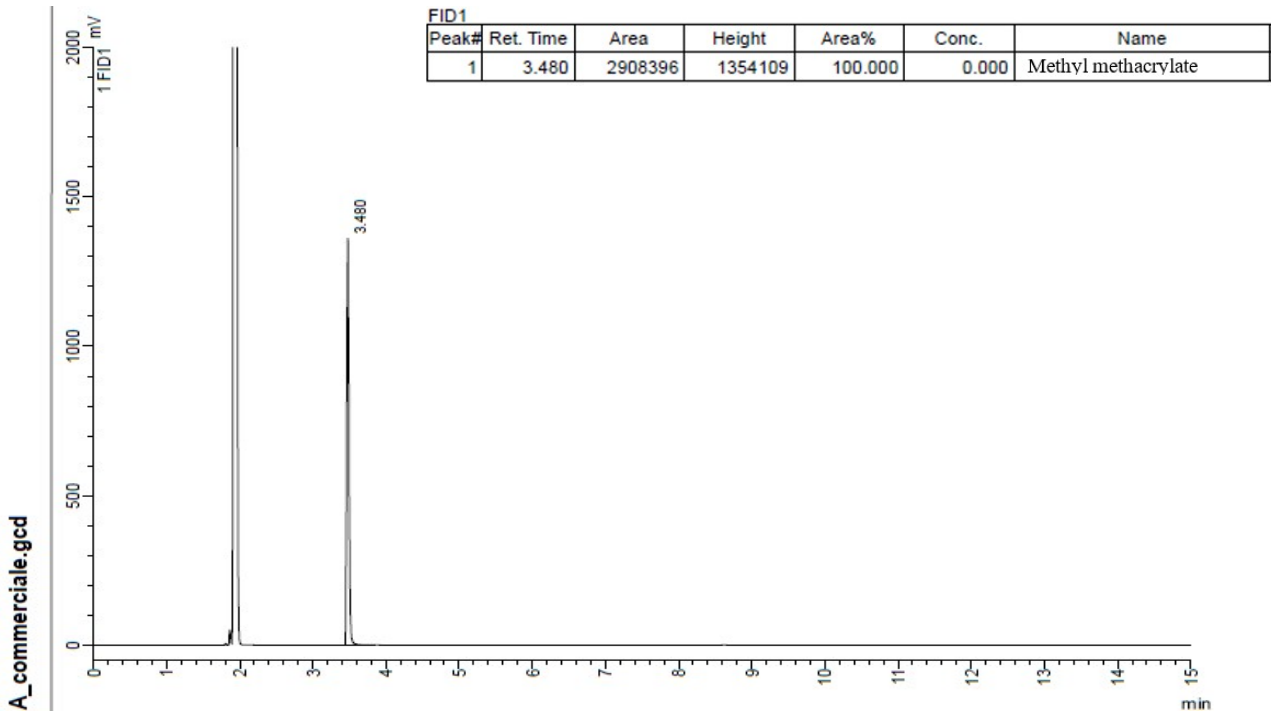

Figure S1. GC-FID chromatogram of the synthetic MMA employed for the production of PMMA-based LSC. The name of the analyte was assigned according to a GC/MS analysis.

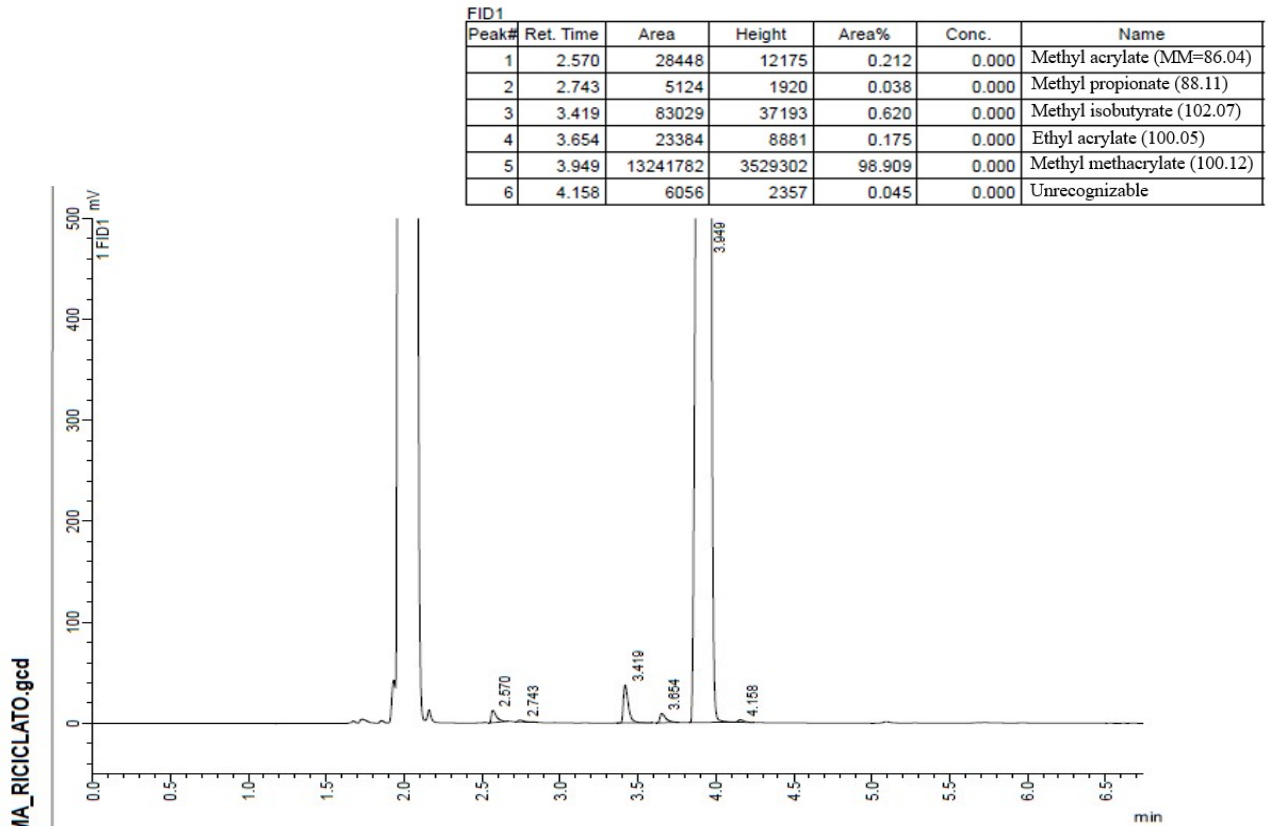

Figure S2. GC-FID chromatogram of the regenerated MMA employed for the production of r-PMMA-based LSC. The name of the analytes was assigned according to a GC/MS analysis.

NMR

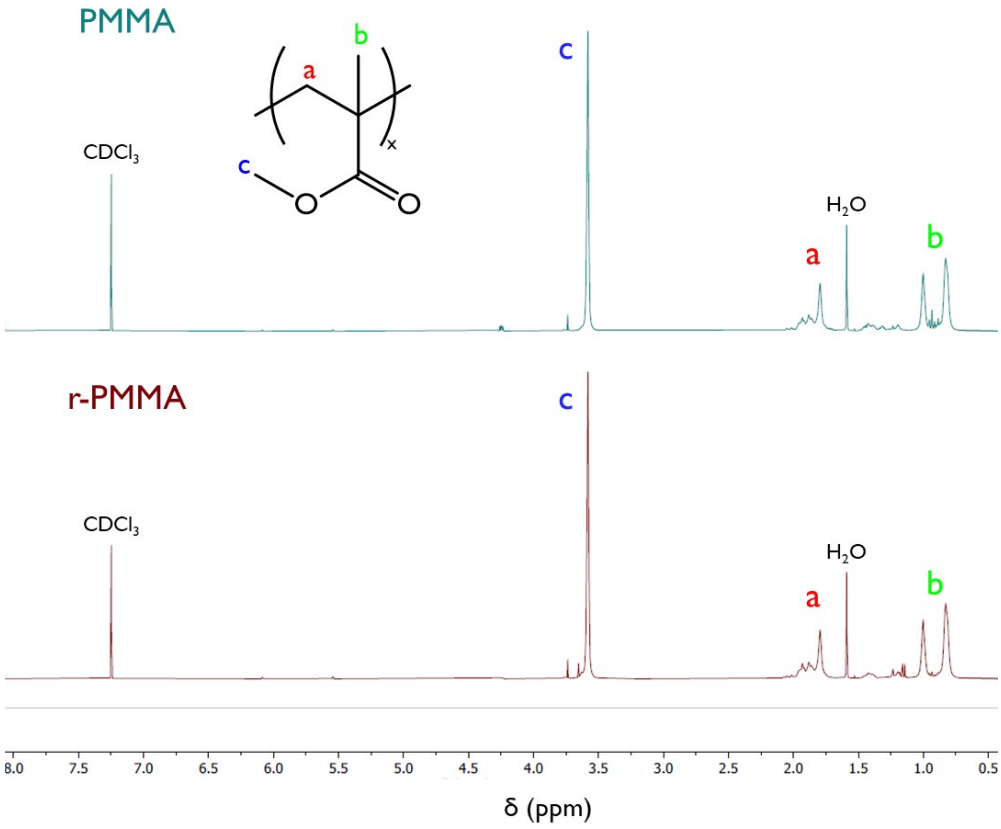

Figure S3: NMR spectra of undoped PMMA and r-PMMA samples.

FT-IR

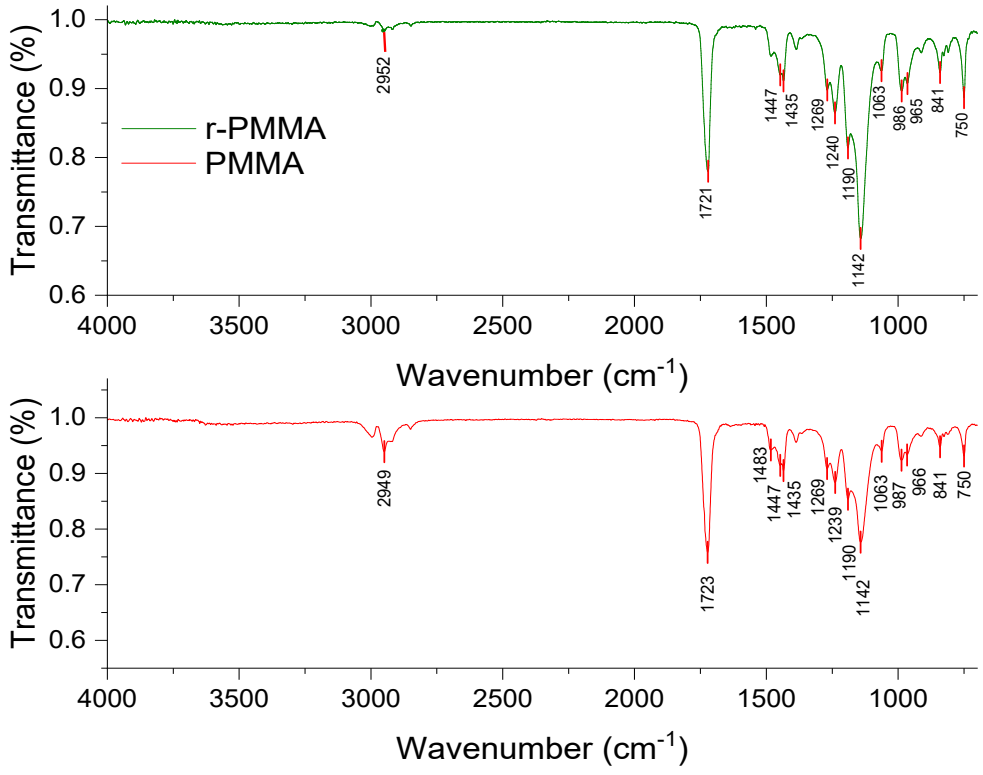

Figure S4: FT-IR (ATR mode) spectra of undoped PMMA and r-PMMA samples.

GPC analysis

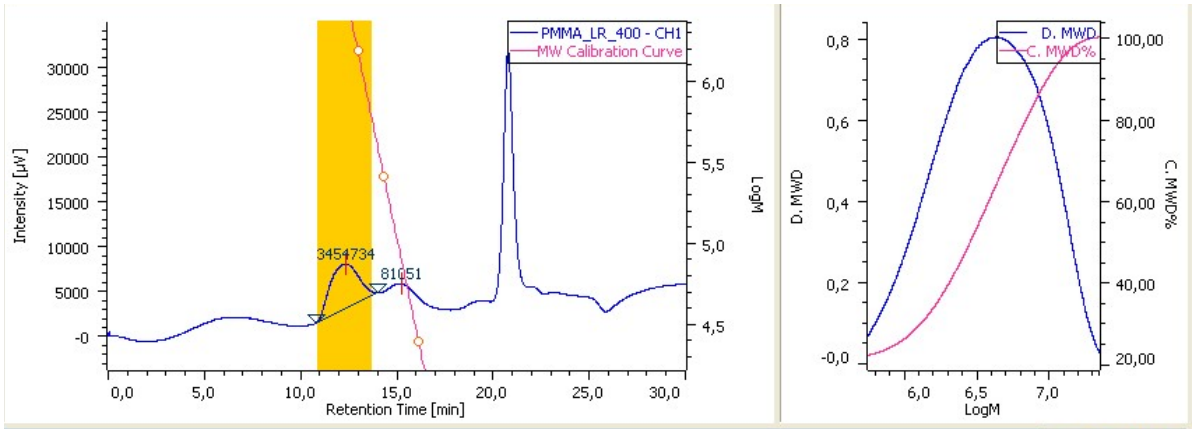

MW Calculation Results: PMMA_LR_400

#	Range	CH	Baseline Range	tR	Mp	Mn	Mw	Mz	Mv	Mw/Mn	Mz/Mw	Range Value	Percentage	Warning
1	10,9000 - 13,7000	1	10,8000 - 14,0000	12,3167	3454734	2806742	5061524	7928799	5061524	1,8033	1,5665	512782	77,62	Extrapc
2	14,2500 - 16,5500	1	13,9500 - 17,1000	15,1833	81051	55139	84793	120285	84793	1,5378	1,4186	147813	22,38	Extrapc

Figure S5. Gel Permeation Chromatogram of a PMMA/LR305 LSC sample showing the bimodal distribution of molecular weights, one from the pre-polymer, the other from the in-situ synthesized macromolecules.

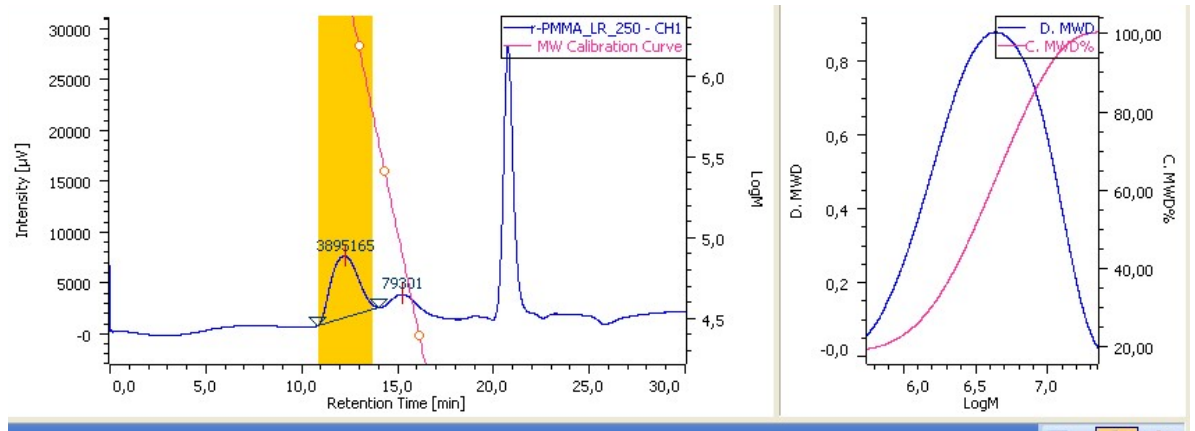

MW Calculation Results: r-PMMA_LR_250

#	Range	CH	Baseline Range	tR	Mp	Mn	Mw	Mz	Mv	Mw/Mn	Mz/Mw	Range Value	Percentage	Warning
1	10,9000 - 13,7000	1	10,8000 - 14,0000	12,2250	3895165	2889959	5041907	7743777	5041907	1,7446	1,5359	592156	80,57	Extrapc
2	14,2500 - 16,5500	1	13,9500 - 17,1000	15,2000	79301	52504	81030	115435	81030	1,5433	1,4246	142769	19,43	Extrapc

Figure S6. Gel Permeation Chromatogram of a r-PMMA/LR305 LSC sample showing the bimodal distribution of molecular weights, one from the pre-polymer, the other from the in-situ synthesized macromolecules.

Thermal analysis – DSC

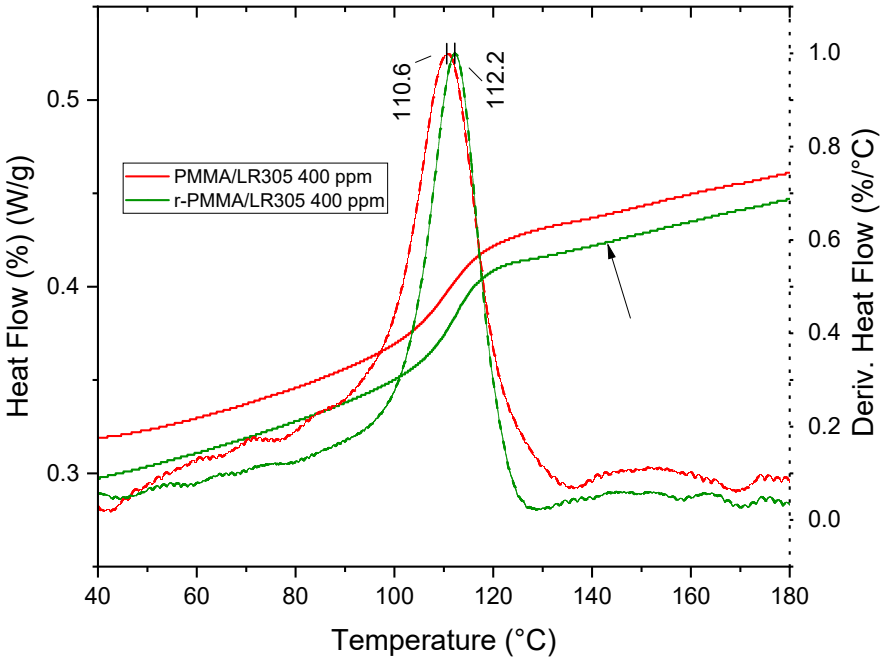

Figure S7. DSC curves (solid) of a PMMA (red) and a r-PMMA (green) samples. Dashed lines represent the heat flow derivatives for PMMA (red) and r-PMMA (green) samples. Glass transition temperatures labeled.

Mechanical tests

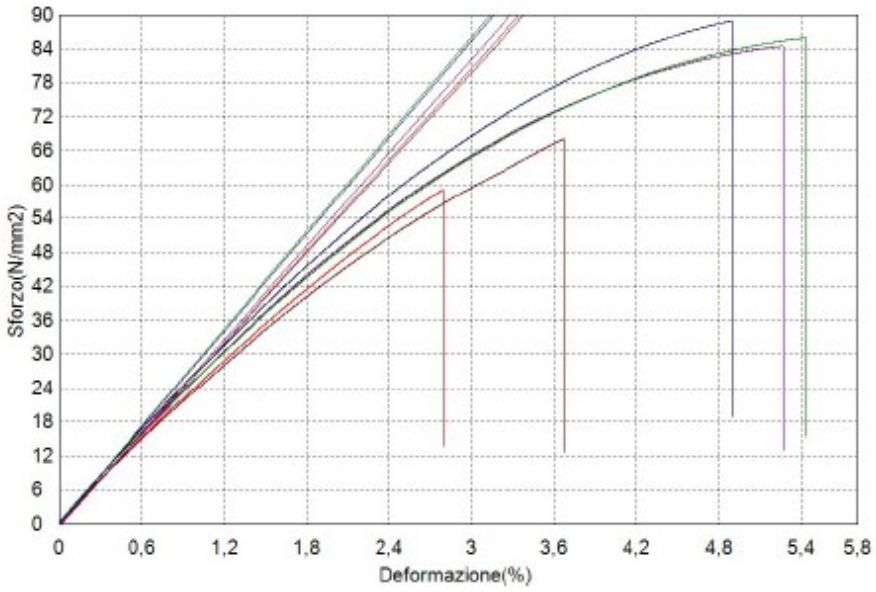

Figure S8. Stress-strain curves of five samples of PMMA.

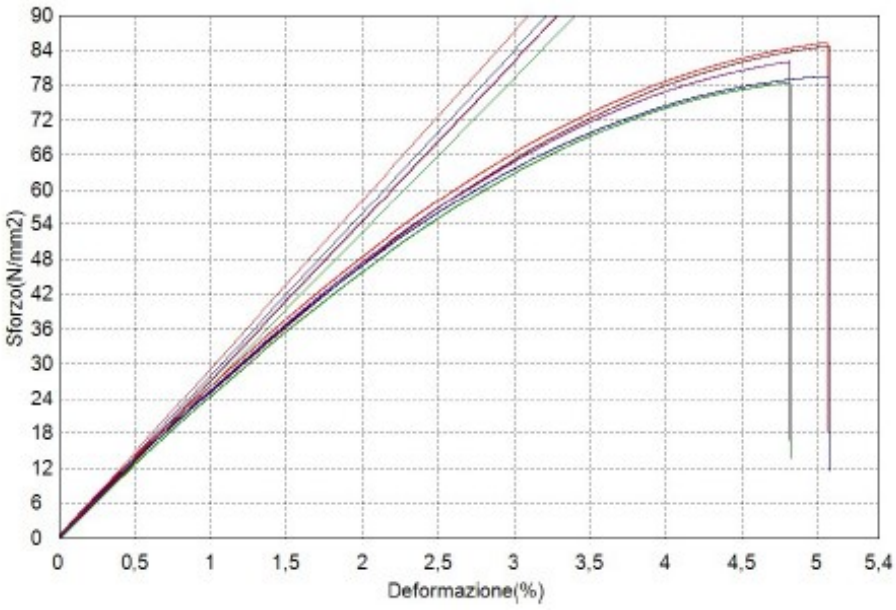

Figure S9. Stress-strain curves of five samples of r-PMMA.

UV-vis transmittance spectra of transparent matrices

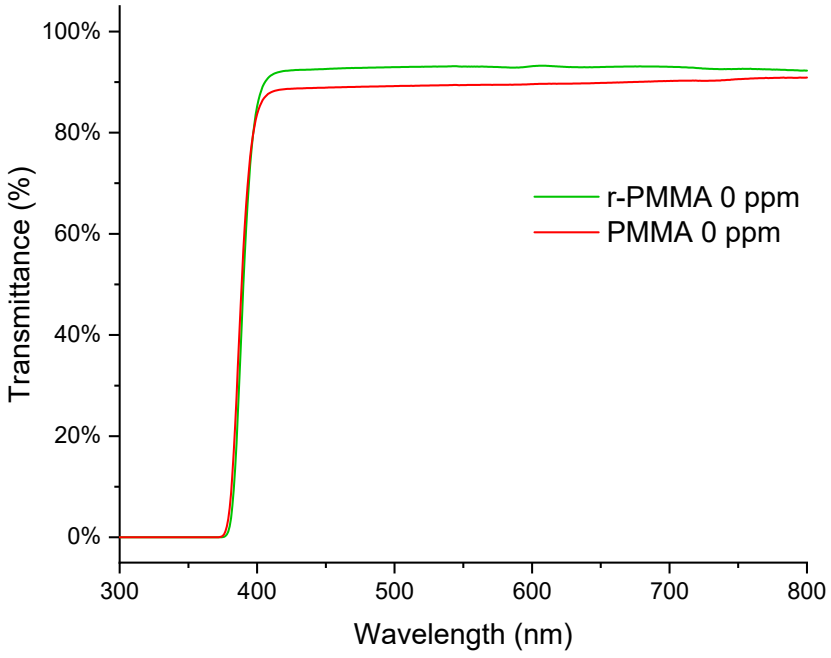

Figure S10. UV-vis transmittance spectra highlighting the high visible light transparency of PMMA (red) and r-PMMA (green) polymer matrices at 0% fluorophore concentration (thickness = 3 mm).

Thermal desorption-GC/MS

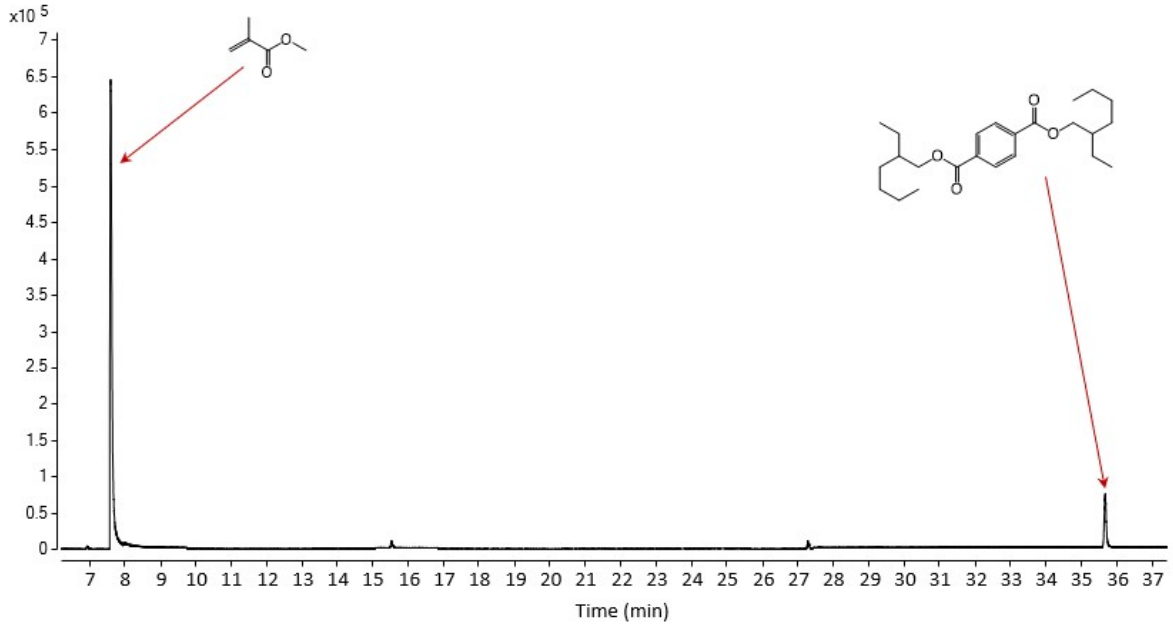

Figure S11. Thermal desorption-GC/MS chromatogram of a PMMA sample.

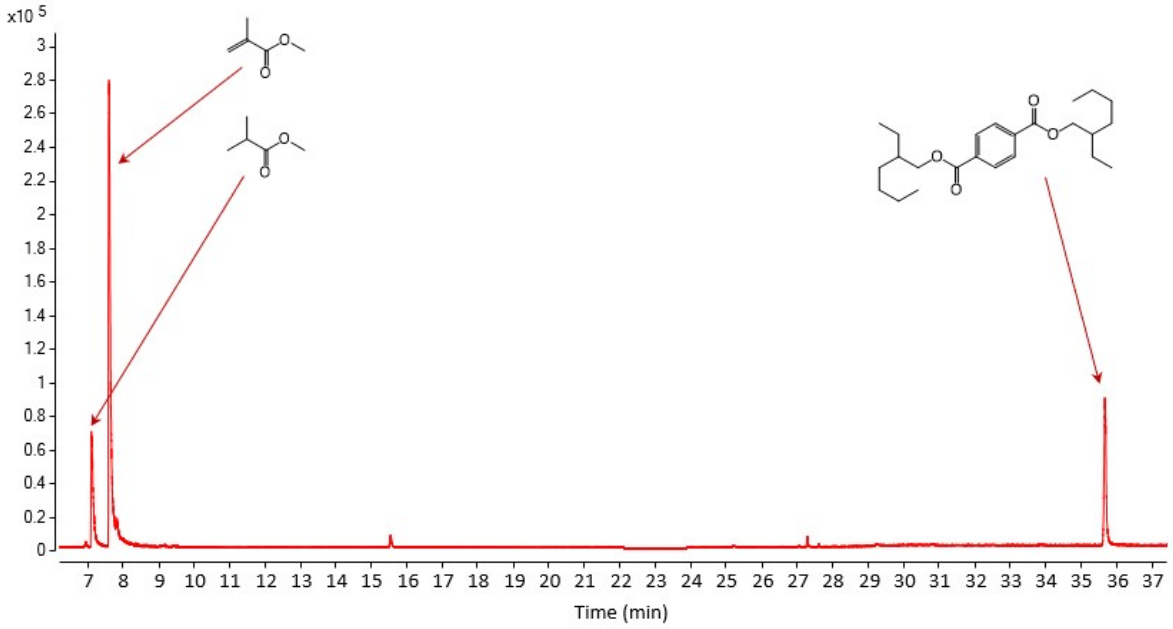

Figure S12. Thermal desorption-GC/MS chromatogram of a r-PMMA sample. A methyl isobutyrate peak appeared at around 7 min.

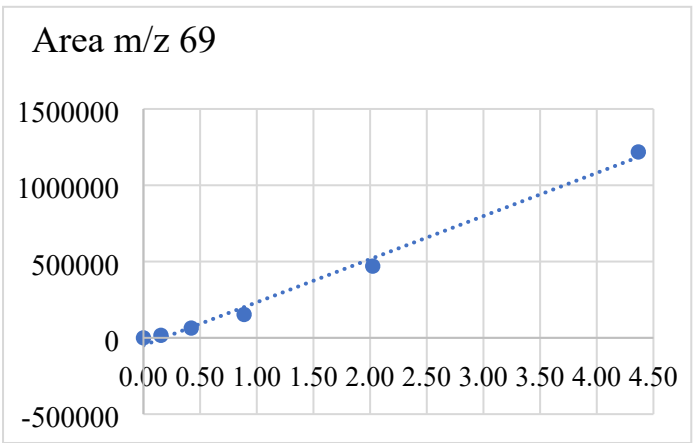

Camp	Conc. m/z 69 (%)
PMMA r1	1.27
PMMA r2	1.16

R-PMMA r1	0.70
R-PMMA r2	0.66

Figure S13. Calibration curve with an MMA standard (on the left) for the residual monomer quantification by Thermal-desorption GC/MS (on the right).

UV-vis and fluorescence spectra

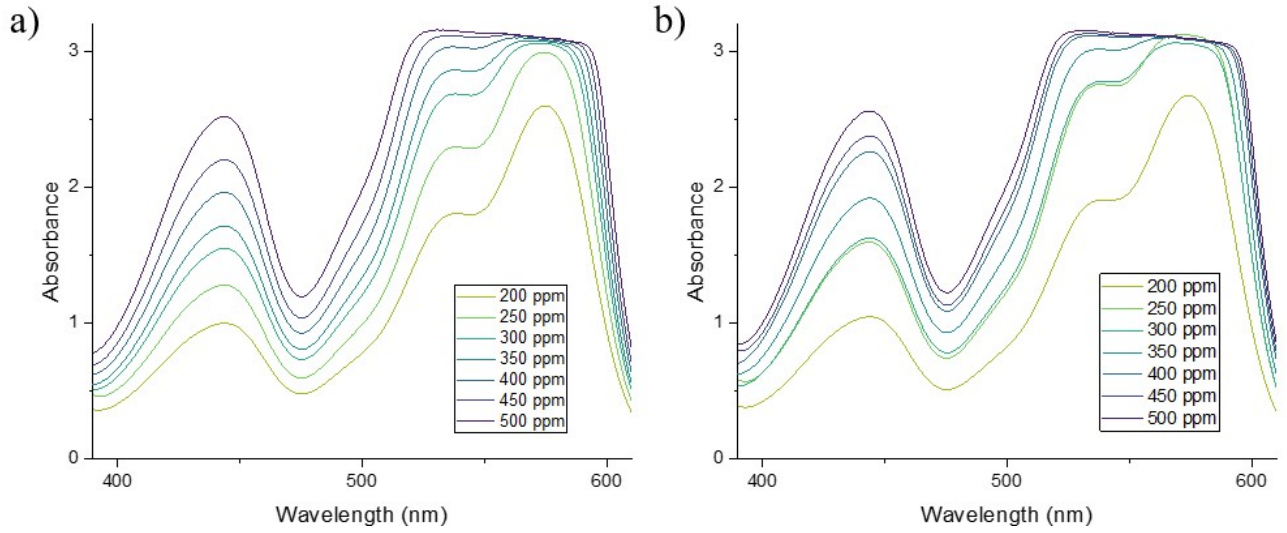

Figure S14. UV-vis absorption spectra of LSC samples (thickness: 3 mm) vs LR305 concentration: a) r-PMMA; b) PMMA.

Epifluorescence microscopy

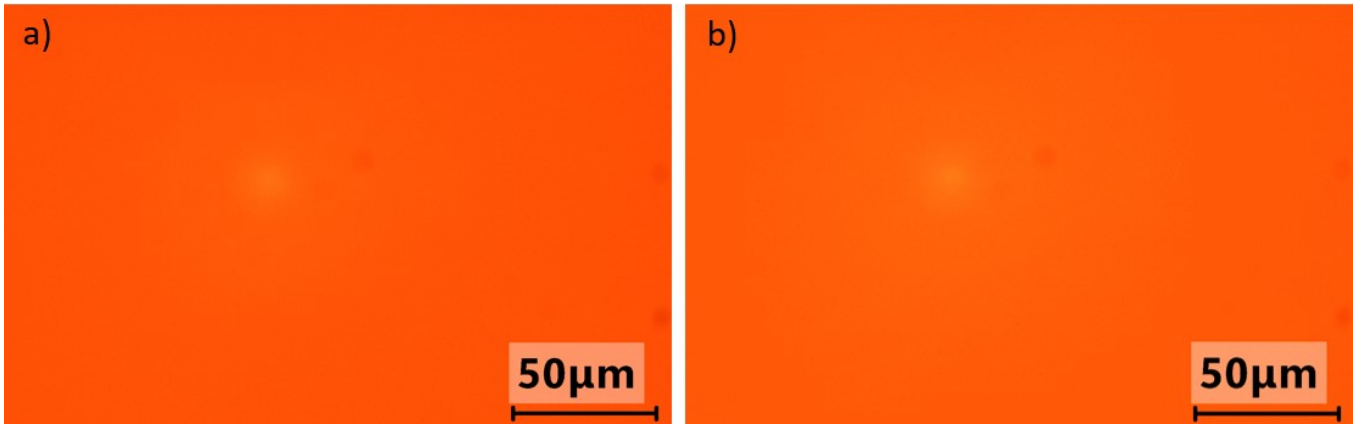

Figure S15. Epifluorescence microscopy images of a) PMMA-LR305 450 ppm LSC; b) r-PMMA-LR305 450 ppm LSC.

UV-vis reflectance spectra of transparent matrices

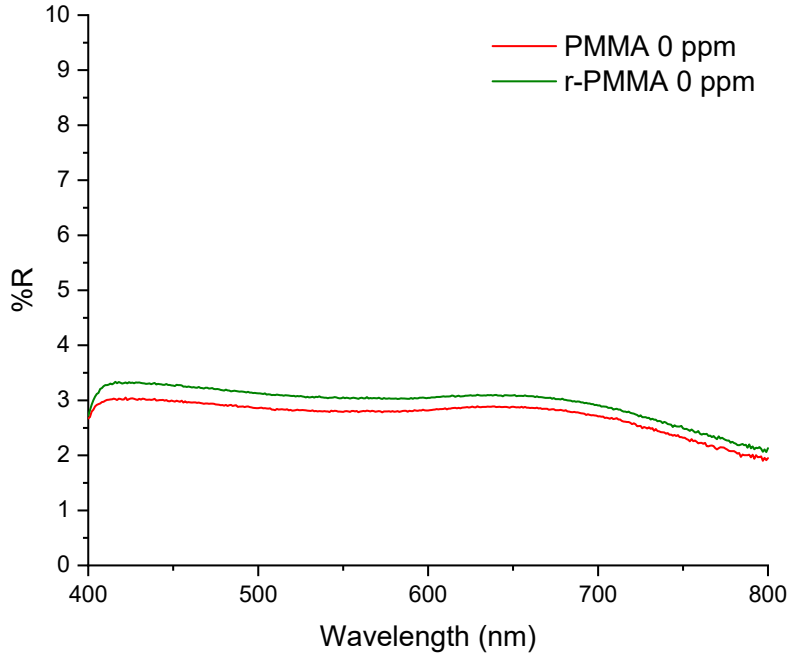

Figure S16. UV-vis reflectance spectra highlighting the same behaviour of PMMA (red) and r-PMMA (green) polymer matrices at 0% fluorophore concentration (thickness = 3 mm).

LSC absorption efficiency

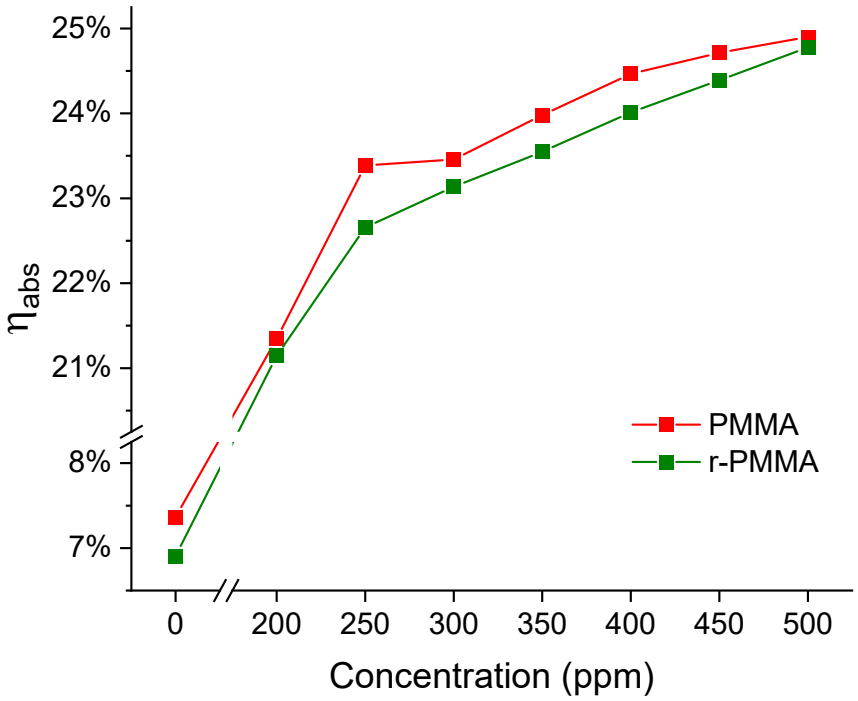

Figure S17. Absorption efficiency η_{abs} versus fluorophore concentration for both PMMA and r-PMMA LSCs.

The LSC absorption efficiency η_{abs} was calculated as the ratio between the external and the internal photonic efficiencies (η_{ext} and η_{int}). See "Electrical and photonic efficiencies determination" section for details.

$$\eta_{abs} = \frac{\eta_{ext}}{\eta_{int}} = \frac{no.\ of\ absorbed\ photons}{no.\ of\ incident\ photons}$$

Eco-profiling calculations

Madreperla S.p.a. data were extracted from GreenCast Environmental Product Declaration (EPD). The same method of impact estimation (EN15804+A2 1.02) was used for calculations for MMA and PMMA production processes, using data retrieved from the Plastics Europe Life Cycle Inventory dataset.

For silicon panels impact calculations we considered:

- Impact of a silicon photovoltaic panel production in Europe[1]: 406 kg CO_2-eq/kWp
- Surface/peak power ratio for silicon PV panels[2]: 5.052 m^2/kWp
- Impact of a 20 x 20 x 0.5 cm^3 LSC production: 2.592 kg CO_2-eq/LSC

Real solar exposition photodegradation test

A r-PMMA sample containing 400 ppm of LR305 was left under solar irradiation and weathering as shown in Figure S11. After 4 months, the sample was characterized as described below (Figure S19) to determine their external photonic efficiencies.

Figure S18. a) Photograph of the solar exposition for photodegradation tests; b) Location of the photodegradation test.

Accelerated photodegradation test

The experiment were conducted for more than 650 minutesat a constant upper surface temperature of 70 °C on the LR305-containing PMMA and r-PMMA slabs (400 ppm). Wishing to comply with the ASTM G154 standard[3] a home-made setup was used, which was composed of a LED tower (Cicci research s.r.l., Grosseto, Italy) as light source and an optical fiber connected to a spectroradiometer as the detector (CCARK.A.4.Spectroradiometer, Fiber Optic VIS/NIR spectrometer, 2048 pixels, grating VA(360-1100nm), slit-50, OSC, DCL- UV/VIS), placed at a distance of < 1 cm from the polymer sample with a detection angle of ca. 35° (Figure S12). The sample was placed on a controllable hot stage (originally used to conduct spatially resolved photoluminescence tests with a thermal module) to adjust its temperature during the experiment. The hot stage was set at 80°C, so as to reach a constant temperature of 70°C on the upper surface of the sample.

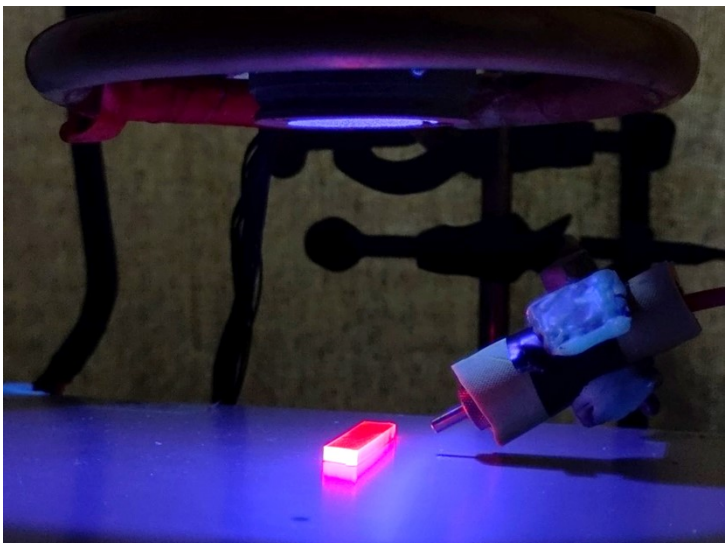

Figure S19. Photograph of the home-built setup used for the accelerated ageing experiment.

The experimental temperature was set directly using the hot stage control and was checked by means of a K-Type thermocouple thermometer in contact with the top surface of the sample. During the experiment, the entire setup was covered with a dark blanket to exclude the external radiation.
As incident light sources, two of the LEDs, named "Far UV" and "UV", were selected (95% irradiation in the 361-406 nm range). Their emission was calibrated with an integrating sphere, which was placed at the same distance from the source as that of the sample. After adjusting the LED intensity, we measured an irradiance of 39.28 W/m^2 in the selected area, to be compared with that of the AM 1.5G solar irradiation (33.45 W/m^2). The measurement thus took place at 1.14 Sun irradiation conditions.

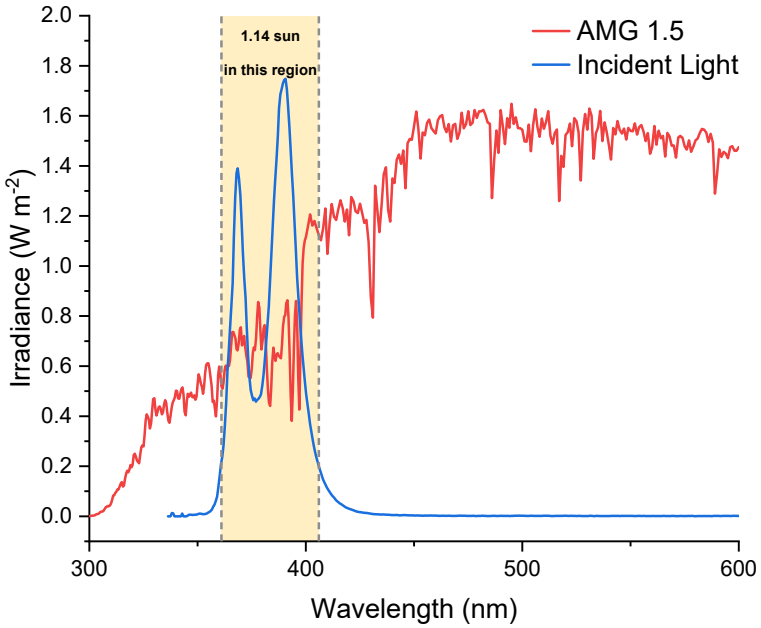

Figure S20. Emission spectrum of the light source used for the photostability experiment, compared to the AM 1.5G spectrum. The area integrated to determine the spectral flux is highlighted in orange.

Electrical and photonic efficiencies determination

Laboratory measurements to determine photonic efficiencies were performed by using a commercially available system (Arkeo – Cicci research s.r.l.) containing a CMOS-based spectrometer with a symmetrical Czerny-Turner optical bench connected to an integrating sphere. As an illumination source an ORIEL® LCS-100 solar simulator 94011A S/N: 322 was utilized under controlled illumination (1 sun, AM 1.5G). An integrating sphere of 5 cm of diameter and 1 cm of aperture is placed along the edge of the glass plate. To avoid the collection of the stray light, the sphere was covered by a black tape with a rectangular aperture as thick as the LSC. The spectrally-resolved edge output photon count was collected from the CMOS-based spectrometer, calibrated into optical power (W) and then in irradiance. Aimed at limiting reflections of unabsorbed light, an absorbing matte black background was placed in contact with the LSC rear side.

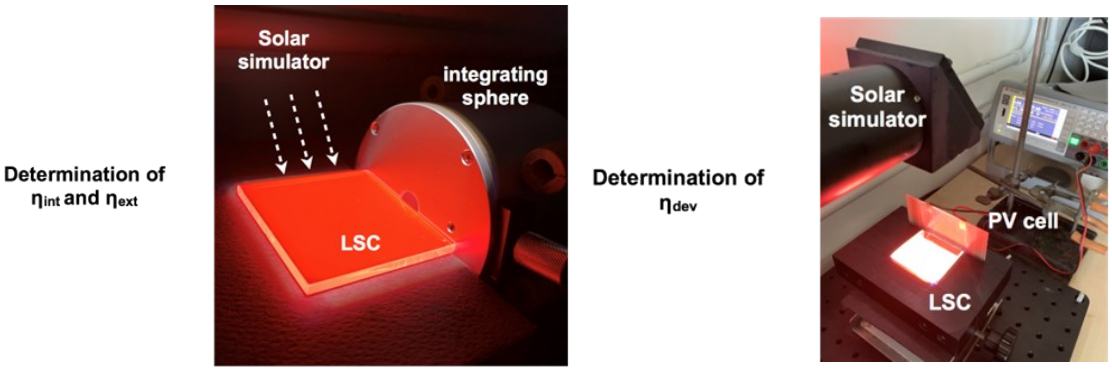

Figure S21: Photos of the experimental setup utilized for the determination of the photonic and device efficiencies.

The optical performances of LSC were evaluated in terms of the internal and the external photon efficiency (η_{int} and η_{ext}, respectively). η_{int} and η_{ext} were calculated from the equations S1 and S2[4,5]:

$$\eta_{int} = \frac{\text{no. of edge} - \text{emitted photons}}{\text{no. of total absorbed photons}} = \frac{\sum_{i=1}^{i=n}\int_{\lambda_1}^{\lambda_2} P_{out,i}(\lambda)\frac{\lambda}{hc}d\lambda}{\int_{\lambda_1}^{\lambda_2} P_{abs}(\lambda)\frac{\lambda}{hc}d\lambda} = \frac{\sum_{i=1}^{i=n}\int_{\lambda_1}^{\lambda_2} P_{out,i}(\lambda)\frac{\lambda}{hc}d\lambda}{\int_{\lambda_1}^{\lambda_2} (P_{in}(\lambda) - P_{tr}(\lambda))\frac{\lambda}{hc}d\lambda} \quad \text{(S1 eq.)}$$

$$\eta_{ext} = \frac{\text{no. of edge} - \text{emitted photons}}{\text{no. of total incident photons}} = \frac{\sum_{i=1}^{i=n}\int_{\lambda_1}^{\lambda_2} P_{out,i}(\lambda)\frac{\lambda}{hc}d\lambda}{\int_{\lambda_1}^{\lambda_2} P_{in}(\lambda)\frac{\lambda}{hc}d\lambda} \quad \text{(S2 eq.)}$$

Where:

a) For edge-emitted photons, n = 4, λ_1 = 400 nm and λ_2 = 800 nm. In the case of incident photons, λ_1 = 300 nm and λ_2 = 1100 nm. For absorbed photons, λ_1 = 350 nm and λ_2 = 610 nm, matching the fluorophore absorption spectrum;

b) the number of edge-emitted photons was obtained from the sum of the output power spectra measured for each edge of the LSC;

c) the number of total absorbed photons was obtained as shown in Eq. S1 from the absorbed power spectrum, derived from the difference between the power spectra of the incident light and the power transmitted by the LSC.

d) The total number of photons incident on the front surface of the LSC was obtained from the input power spectrum of the light source incident on the illuminated surface area of the LSC.

The input irradiation (power density) of the solar simulator light source incident on the LSC is shown in Figure S4. The integrated power was equal to 78 mW/cm^2.

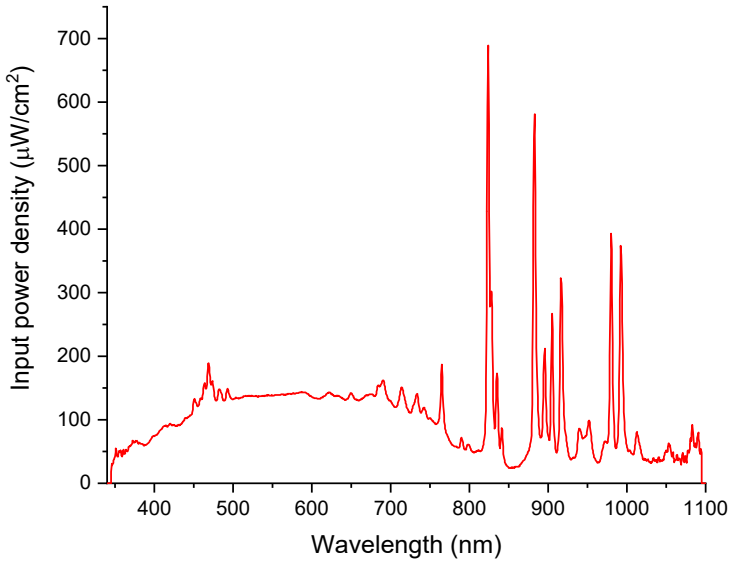

Figure S22: Input power density of the light source incident on the illuminated surface area of the LSC, Pin(λ)

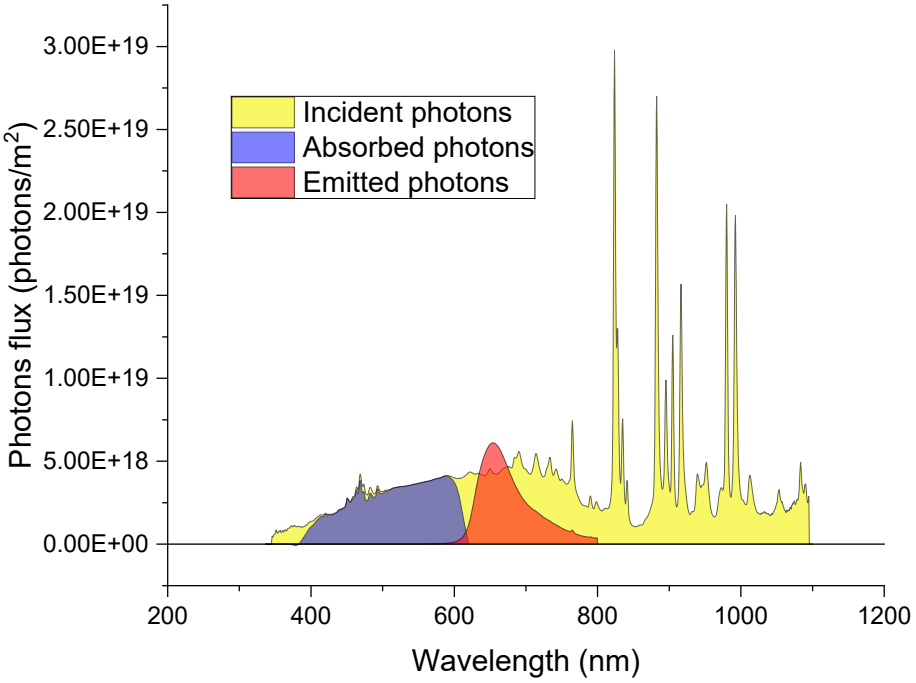

Figure S23: Incident (yellow), absorbed (blue) and emitted (red) photons flux spectra versus photon wavelength for a r-PMMA/LR305 400 ppm LSC.

The LSC electrical efficiency was determined connecting two Si-PV cells in series to an edge of the thin-film LSCs by using silicone grease. The performance of the assembled LSC-PV systems was assessed under standard illumination conditions by measuring the power conversion efficiency of the resulting LSC device (η_{dev}), defined as the electrical power effectively extracted from the PV cells (P^{out}_{el}) relative to the luminous power hitting the top surface of the LSC (P^{in}_{opt}):

$$\eta_{dev} = \frac{P_{el}^{out}}{P_{opt}^{in}} = \frac{FF \cdot I_{SC} \cdot V_{OC}}{P_{opt}^{in} \cdot A_{LSC}} \qquad \text{(S3 eq.)}$$

where FF, I_{SC}, and V_{OC} are the fill factor, short-circuit current, and open-circuit voltage of the edge-mounted PV cells, respectively, A_{LSC} is the front-illuminated area of the LSC device, and P^{in}_{opt} is the incident solar power density expressed in mW cm^{-2}.

For the determination of η_{dev}, two PV cells IXYS KXOB25-12X1F (22 x 7 mm, V_{oc} = 0.69 V, I_{sc} = 46.7 mA, FF > 70%, η = 25%) were connected in series and the current/voltage characteristics determined with a precision source/measure unit (Keysight Technologies B2900 Series)[6]. Silicon was used to grease the LSC edge. The other three edges of the LSC were covered with a reflective aluminium tape. During the measurements, a black matte layer was placed beneath the LSC.

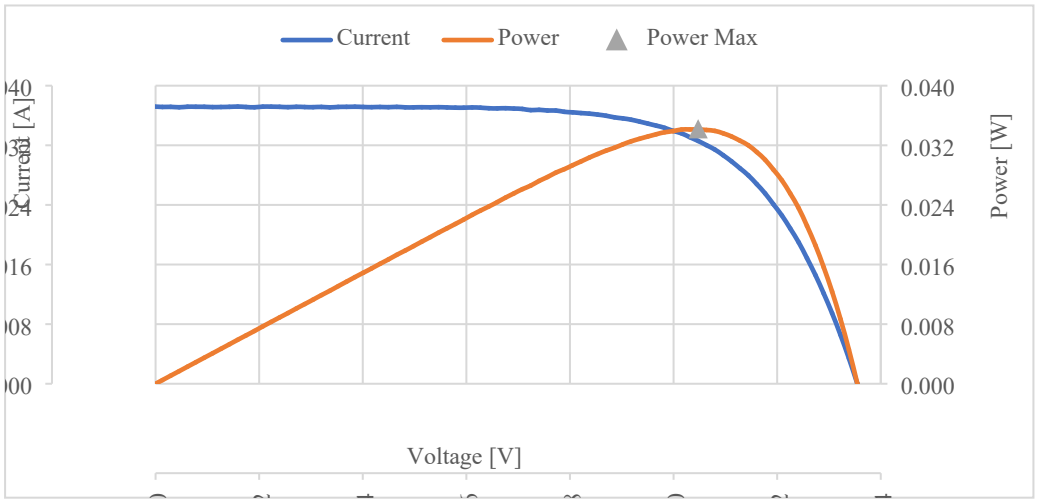

Figure S24. I-V curve of the monocrystalline silicon solar cells (IXOLAR cells).

Concentration	C (PMMA)	C (r-PMMA)
200 ppm	0.399 ± 0.002	0.405 ± 0.001
250 ppm	0.414 ± 0.002	0.420 ± 0.001
300 ppm	0.425 ± 0.001	0.432 ± 0.001
350 ppm	0.409 ± 0.008	0.437 ± 0.004
400 ppm	0.435 ± 0.005	0.461 ± 0.001
450 ppm	0.431 ± 0.001	0.454 ± 0.003
500 ppm	0.420 ± 0.004	0.441 ± 0.002

Table S1. Concentration factors (C) for both c-PMMA and PMMA-based LSCs at various concentrations

References

(1) C. Reichel, A. Müller, L. Friedrich, S. Herceg, M. Mittag, A. Protti, D. H. N. CO2 Emissions of Silicon Photovoltaic Modules – Impact of Module Design and Production Location. *8th World Conf. Photovolt. Energy Convers.* **2022**, No. September, 1617–1619.

(2) Müller, A.; Friedrich, L.; Reichel, C.; Herceg, S.; Mittag, M.; Neuhaus, D. H. A Comparative Life Cycle Assessment of Silicon PV Modules: Impact of Module Design, Manufacturing Location and Inventory. *Sol. Energy Mater. Sol. Cells* **2021**, *230* (July), 111277. https://doi.org/10.1016/j.solmat.2021.111277.

(3) G-154, A. ASTM G-154 Operating Fluorescent Light Apparatus for UV Exposure of Nonmetallic Materials. *West Conshohocken, PA* **2016**, 1–11.

(4) Debije, M. G.; Evans, R. C.; Griffini, G. Laboratory Protocols for Measuring and Reporting the Performance of Luminescent Solar Concentrators. *Energy Environ. Sci.* **2021**, *14* (1), 293–301. https://doi.org/10.1039/d0ee02967j.

(5) Yang, C.; Atwater, H. A.; Baldo, M. A.; Baran, D.; Barile, C. J.; Barr, M. C.; Bates, M.; Bawendi, M. G.; Bergren, M. R.; Borhan, B.; Brabec, C. J.; Brovelli, S.; Bulović, V.; Ceroni, P.; Debije, M. G.; Delgado-Sanchez, J.-M.; Dong, W.-J.; Duxbury, P. M.; Evans, R. C.; Forrest, S. R.; Gamelin, D. R.; Giebink, N. C.; Gong, X.; Griffini, G.; Guo, F.; Herrera, C. K.; Ho-Baillie, A. W. Y.; Holmes, R. J.; Hong, S.-K.; Kirchartz, T.; Levine, B. G.; Li, H.; Li, Y.; Liu, D.; Loi, M. A.; Luscombe, C. K.; Makarov, N. S.; Mateen, F.; Mazzaro, R.; McDaniel, H.; McGehee, M. D.; Meinardi, F.; Menéndez-Velázquez, A.; Min, J.; Mitzi, D. B.; Moemeni, M.; Moon, J. H.; Nattestad, A.; Nazeeruddin, M. K.; Nogueira, A. F.; Paetzold, U. W.; Patrick, D. L.; Pucci, A.; Rand, B. P.; Reichmanis, E.; Richards, B. S.; Roncali, J.; Rosei, F.; Schmidt, T. W.; So, F.; Tu, C.-C.; Vahdani, A.; van Sark, W. G. J. H. M.; Verduzco, R.; Vomiero, A.; Wong, W. W. H.; Wu, K.; Yip, H.-L.; Zhang, X.; Zhao, H.; Lunt, R. R. Consensus Statement: Standardized Reporting of Power-Producing Luminescent Solar Concentrator Performance. *Joule* **2022**, *6* (1), 8–15. https://doi.org/10.1016/j.joule.2021.12.004.

(6) Yang, C.; Liu, D.; Lunt, R. R. How to Accurately Report Transparent Luminescent Solar Concentrators. *Joule* **2019**, *3* (12), 2871–2876. https://doi.org/10.1016/j.joule.2019.10.009.